Search for thermal X-ray radiation from hot polar cap in pulsars

Janusz Gil
Andrzej Szary, Giorgi Melikidze

Kepler Institute of Astronomy
University of Zielona Góra, Poland

June 14, 2014

Simplest pulsar toy model

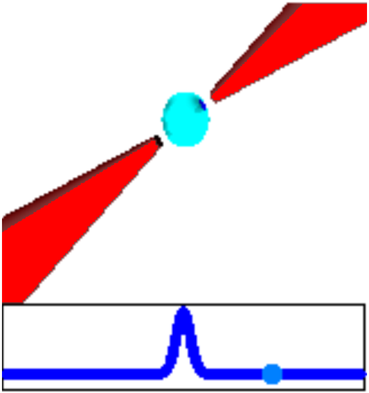

Two beams originating above two opposite Polar Caps

Pulse observed when at least one of them hits the Earth

Observations clearly show that each beam has complicated and dynamic structure

More detailed toy model needed

Pulsar carousel model (see next slide)

Toy pulsar model: Spark „Carousel”

Spark associated subpulse radio sub-beams

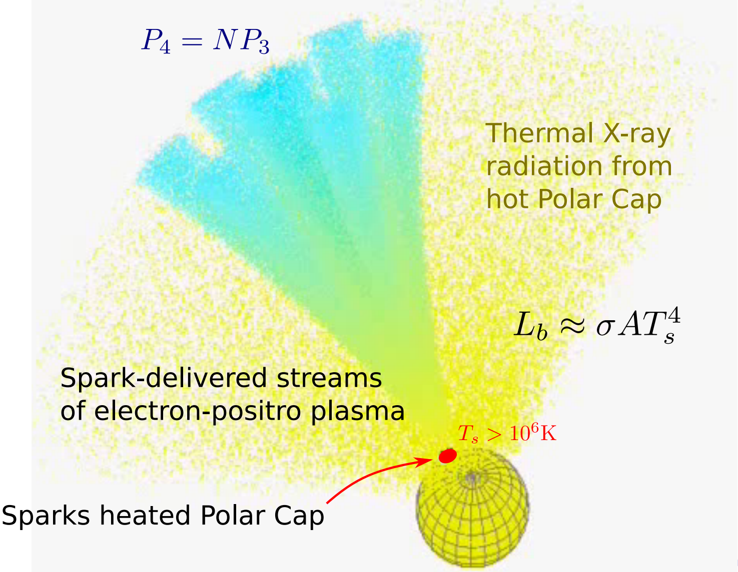

Co-rotating magnetosphere

$E_c = -(\Omega \times r/c) \times B_s$ force-free magnetosphere

$E_c \cdot B_s = 0 \quad \Delta V_{\|}$ (GJ69, RS75)

No acceleration along B (no radio emission?)

$\rho_c = \rho(1/2\pi)\mathrm{div} E_c = \rho_{\mathrm{GJ}}$ Co-rotating charge density

$= -\Omega \cdot B/(2\pi c) = \pm B_s/cP$

$v_{\mathrm{cor}} = c(E_c \times B_s)/B^2 = cE_c/B_s$ Linear co-rotation velocity

$$v_{\mathrm{dr}} = c(\Delta E \times B_s)/B^2 = c\Delta E_c/B_s$$

Non-corotation -> deviation from the GJ charge density ($\rho < \rho_c = \rho_{\mathrm{GJ}}$)

Non-corotation

Pulsar radiation requires acceleration of charged particles along magnetic field lines $\rightarrow$ electric field along field lines $\rightarrow$ deviation from GJ charge density $\rightarrow$ NON-COROTATION

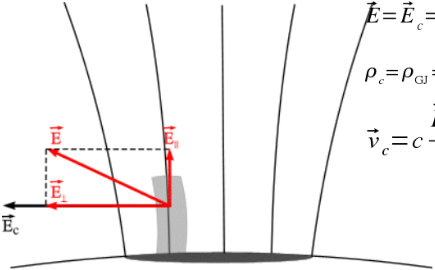

$$\vec{E}=\vec{E}_c=\frac{1}{c}\vec{B}_s\times(\vec{\Omega}\times\vec{r})$$

$$\rho_c=\rho_{\rm GJ}=-\frac{(\vec{\Omega}\cdot\vec{B}_c)}{cP}$$

$$\vec{v}_c=c\,\frac{\vec{E}_c\times\vec{B}_s}{B_s^2}$$

$$\vec{E}=\vec{E}_{||}+\vec{E}_{\perp} \qquad \Delta\vec{E}_{\perp}=\vec{E}_c-\vec{E}_{\perp}$$

$$\rho=(1-\eta)\rho_{\rm GJ};\ \ \eta<<1 \qquad \vec{v}_{\rm df}=c\,\frac{\Delta\vec{E}_{\perp}\times\vec{B}_s}{B_s^2}$$

Evidence of NON-COROTATION should be clearly present in pulsar data in form of some consistent drift motion of pulse constituents (subpulses)

Sub-pulse drift

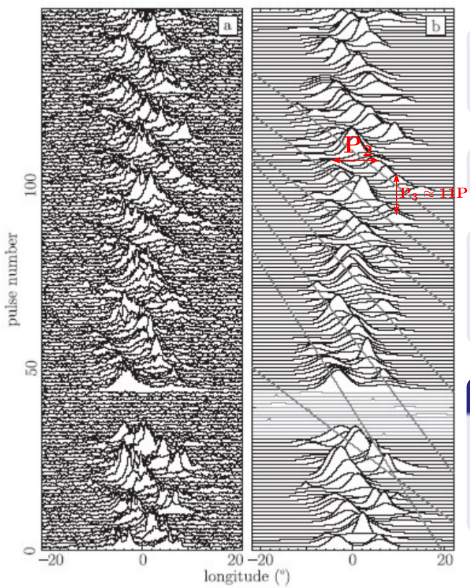

Line-of-sight (l-of-s) grazing the overall pulsar beam

Apparent subpulse drift-bands

Modulation of intensity along drift-bands consistent with carousel model

that is

Sub-beams seem to continue to circulate beyond the observed pulse-window

(after van Leuven, Stappers et al.)

Carousel Model

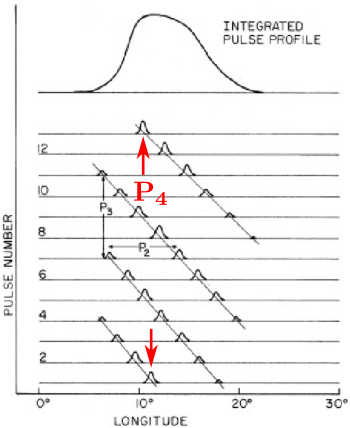

FIG. 5.—Schematic (after Backer 1973) of integrated pulse profile, arrival times of individual pulses, and definition of P_2, P_3 for those pulsars showing the "drifting subpulse" phenomenon. Arrival times of individual pulses are given in terms of a longitude for which 360° corresponds to the full pulsar period.

(Ruderman & Sutherland 1975)

Apparent drift rate

$D = P_2/P_3$

P_2 - distance between driftbands in longitude

P_3 - distance between driftbands in P_1

Intrinsic drift rate

$P_4 = P_3 N$, N - number of rotating sub-beams

Intrinsic drift rate

P_4 - distance between the same driftbands and time interval to complete one rotation around the pole

very difficult to measure, only 8 cases known !!!

Partially Screened Gap

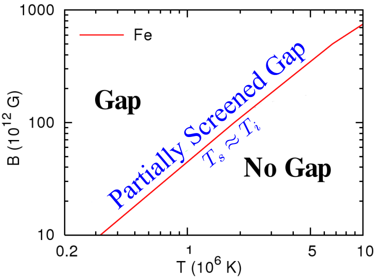

(Medin & Lai 2007)

$$T_i = \epsilon/30k =$$
$$= (7 \times 10^4 \mathrm{K})(B_s/10^{12}\mathrm{G})^{0.7}$$

$$T_s \approx T_i > 10^6 \text{ K}$$

$$\rho_\pm + \rho_{\rm th} = \rho_{\rm GJ}$$

The basic features of the Partially Screened Gap (PSG) model (Gil, Melikidze & Geppert 2003) are as follows:

- Positive charges cannot be supplied at the rate that would compensate the inertial outflow through the light cylinder. As a result, a significant potential drop develops above the polar cap.
- Backflow of electrons heats the surface to temperature above 10^6 K. Thermal ejection of iron ions causes a partial screening of the acceleration potential drop. Consequently, backflow heating decreases as well. Thus heating leads to cooling which is a classical thermostat.
- Surface temperature $T_{\rm s}$ is thermostatically regulated to retain its value close to critical temperature $T_{\rm i}$ above which the thermal ion flow reaches co-rotation limited level (Goldreich-Julian charge density), thus $T_{\rm BB} = T_{\rm s} \approx T_{\rm i}$
- According to calculations of the cohesive energy by Medin & Lai 2007, this can occur if the surface magnetic field is close to 10^{14} G. In majority of radio pulsars this has to be a highly non-dipolar crust anchored field.

Thermal X-ray radiation (the hot spot)

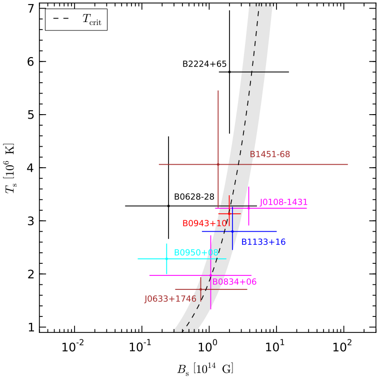

Figure: Surface temperature vs. strength of surface magnetic field. The dashed line corresponds to critical temperature *(Medin and Lai 2008)*.

$$b = \frac{A_{pc}}{A_{BB}}$$

Magnetic flux conservation law

$$B_s = b \cdot B_d \sim 10^{14}\ \mathrm{G},$$

Name	T_{BB} $(10^6 \mathrm{K})$	R_{BB} (m)	R_{pc} (m)	b	B_s $(10^{14}\mathrm{G})$
J0108–1431	3.2	6	161	768	3.9
B0628–28	3.3	64	130	4	0.2
J0633+1746	1.7	62	297	23	0.7
B0834+06	2.0	30	128	18	1.1
B0943+10	3.1	22	138	126	3.2
B0950+08	2.3	42	288	48	0.2
B1133+16	3.2	14	133	96	4.1
B1451–68	4.1	14	282	418	1.4
B2224+65	5.8	28	175	39	2.0

Non-dipolar magnetic field at the polar cap of neutron stars

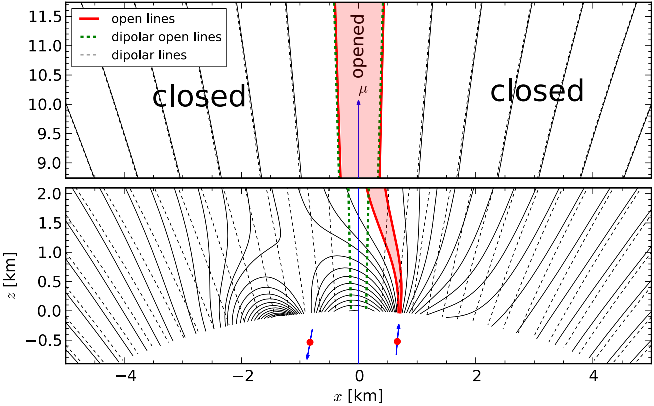

Possible non-dipolar structure of the magnetic field lines". The magnetic field structure was obtained using crust-anchored local anomalies *(Gil et al. 2002, Szary et al. in preparation)*.

"The Hall drift can produce small-scale strong surface magnetic field anomalies (spots)." (Geppert et al. 2013)

X-ray vs. radio

Possible interrelation between radio and X-ray signatures of drifting subpulses in pulsars

$$L_b \text{ versus } P_4$$

Thermal (bolometric) luminosity from polar cap heated by sparks associated with (drifting) subpulses

$$L_b = \sigma T^4 A_{\rm bol} = \sigma T^4 A_{\rm pc}(B_d/B_s)$$

Tertiary (carousel) subpulse drift periodicity $\rightarrow$ circulation period of subpulse associated sparks

$$P_4 \approx 2\pi r_p / v_d$$

X-ray vs. radio

Thermal X-ray luminosity from spark-heated polar cap [erg/s]

$$L_b = 2.5 \times 10^{31} \times (P_{-15}/P^3)(P_4/P)^{-2}$$

Spin-down power

$$\dot{E} = I\Omega\dot{\Omega} \qquad I = I_{45} 10^{45}\ \mathrm{g\,cm^2}$$

Efficiency of thermal radiation from hot PC

$$\boxed{L_b/\dot{E} = (0.63/I_{45})(P_4/P)^{-2}}$$

Intensity of thermal BB radiation is correlated with plasma circulation rate

(acceleration)

L_b - Polar Cap heating rate due to $\Delta E_{\parallel}$

(drift)

P_4 - plasma circulation rate due to $\Delta E_{\perp}$"

Two components of the non-corotation electric field above the Polar Cap

$$\Delta E_{\parallel} \sim \Delta E_{\perp}$$

The Chameleon pulsar (B0943+10)

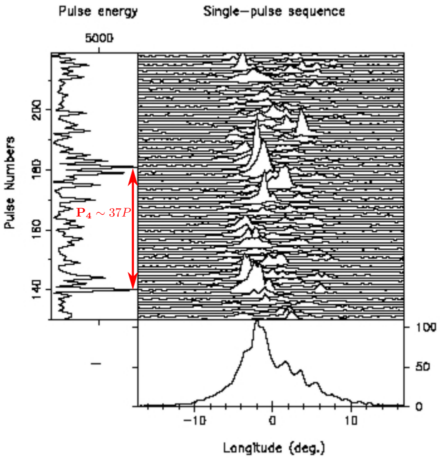

(Deshpande & Rankin 1999)

$P_1 = 1.089$ s

$P_3 = 1.87P$ (primary)

$P_3 = 2.15P$ (aliased)

$P_4 = 37.35P$

Number of sub-beams circulating around B

$N = P_4/P_3 = 20$

Parameters of simultaneous B and Q modes spectral fits (see Table 3 in *(Mereghetti et al. 2013)*)

Model	T_s (MK)	$R_{\rm BB}$ (m)	PL	$N_{\rm h}$ 10^{20} cm^{-2}	$\chi^2_{\rm red}$/dof.
Constant BB and pulsed PL	3.0	21	2.2	2.4	0.99/16

- The power-law model for the B-mode yields a rather steep spectrum (photon index of 4.1)
- An interstellar absorption is larger than that expected based on the total Galactic column density in this direction ($2.3 \times 10^{20}\,{\rm cm}^{-2}$ *(Kalberla et al. 2005)*)

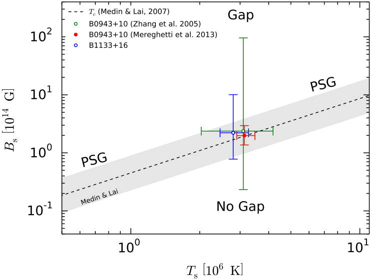

"Study of the remarkable X-ray variability of PSR B0943+10" (300 ks, AO-13, XMM-Newton, Mereghetti et. al)

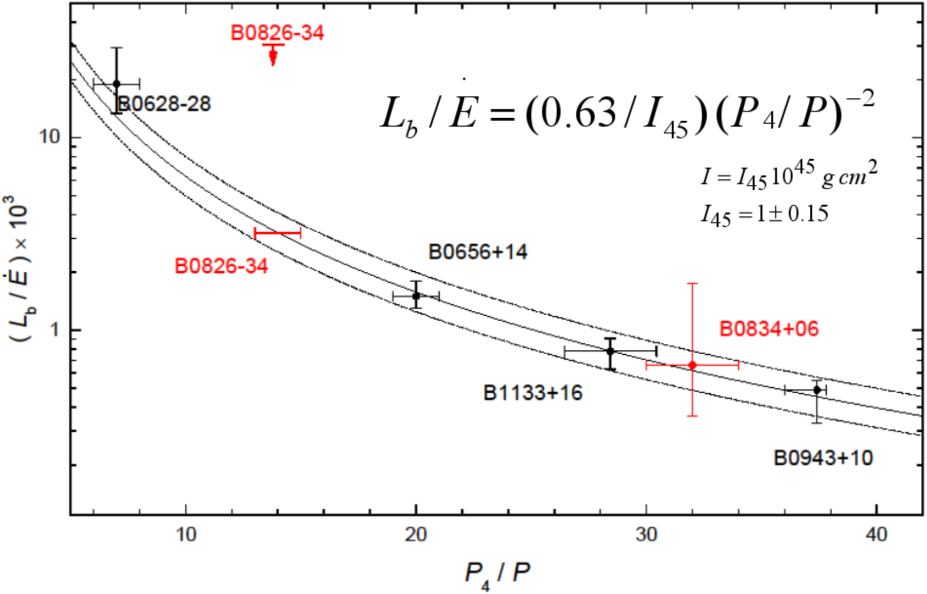
B0826-34
B0628-28
$L_b / \dot{E} = (0.63 / I_{45})(P_4 / P)^{-2}$
$I = I_{45} 10^{45}\ g\ cm^2$
$I_{45} = 1 \pm 0.15$
B0656+14
B0826-34
B0834+06
B1133+16
B0943+10
10
1
$(L_b / \dot{E}) \times 10^3$
10
20
30
40
P_4 / P

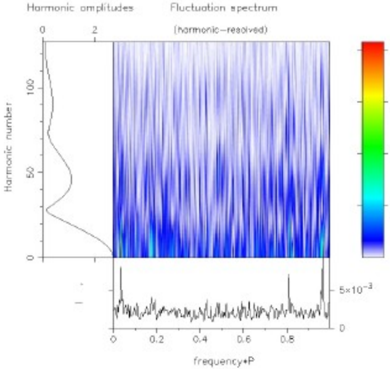

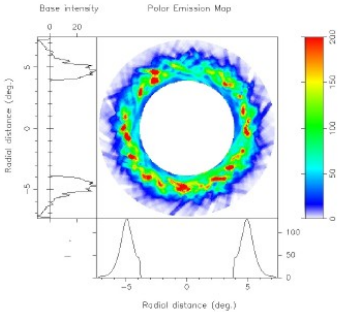

Figure A2. Polar map constructed using pulses 242-504 of the A PS. Here, $\hat{P}_3$ was determined to be 28.44 P_1, so the average of 7 carousel rotations is depicted. The magnetic axis is at the centre of the diagram, the "closer" rotational axis is upward, and (assuming a positive or equatorward traverse) the sightline track sweeps through the lower part of the pattern. Here, the star would rotate clockwise, causing the sightline to cut the counter-clockwise-rotating subbeam pattern from right to left; see DR01 for further details. The side panels give the "base" function (which has not been subtracted from the map), and the lower panel shows the radial form of the average beam pattern.

$$P_4 = 28.44 P_1$$

$$P_3 = (1.237 \pm 0.011) P_1$$

$$N = P_4/P_3 = 22.991 \pm 0.01 = 23$$

(Rankin et al. 2007)

23 sub-beams!

The past: "X-ray emission from the nearby PSR B1133+16..." *(Kargaltsev et al. 2006)*

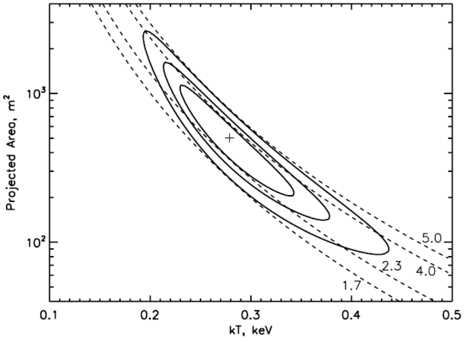

FIG. 4.—Confidence contours (68%, 90%, and 99%, computed for two interesting parameters) for the PL (*top*) and BB (*bottom*) model fits to the ACIS spectrum of PSR B1133+16. The PL normalization is in units of 10^{-6} photons cm^{-2} s^{-1} keV^{-1} at 1 keV. The BB normalization (*vertical axis*) is the projected emitting area in units of m^2, for $d = 357$ pc. The lines of constant unabsorbed flux (PL model; in units of 10^{-14} ergs cm^{-2} s^{-1}) and constant bolometric luminosity (BB model; for $\langle\cos\theta\rangle = 1$, in units of 10^{28} ergs s^{-1}) are plotted as dashed lines, for fixed $N_{\rm H} = 1.5\times10^{20}$ cm^{-2}.

(Kargaltsev et al. 2006).

$P = 1.188\ \mathrm{s},\ \dot{P}_{-15} = 3.73$

PSR B1133+16 was observed in Feb. 2005 by the Chandra ACIS instrument for an exposure of $\sim$ 18 ks.

$A_{\rm pc} \approx 5.5 \times 10^4 m^2 \quad A_{\rm BB} \approx 5 \times 10^2 m^2$

$$A_{\rm pc} \approx 100 A_{\rm BB}$$

Because of the small number of counts detected (33 within the source extraction aperture), the spectrum did not allow to differentiate between models like powerlaw or blackbody.

The future: "A simultaneous X-ray and radio observation of the nearby pulsar B1133+16" (Gil et. al)

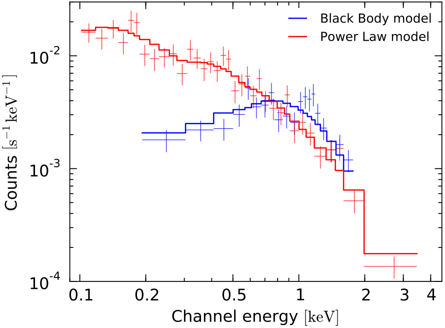

Simulated EPIC-pn spectra assuming a black-body (blue points) or powerlaw (red points). The assumed exposure time is 100 ks. *(The XMM-Newton proposal, Gil et al.).*

X-ray observations: five observing sessions with XMM-Newton, 146 ks in total

- 25th May (**25 ks**)
- 31st May (**23 ks**)
- 14th June (**38 ks**)
- 22nd June (**35 ks**)
- 28th June (**25 ks**)

Simultaneous radio observations

- GMRT - **315 MHz**
- Effelsberg - **5 GHz**
- LOFAR - **100 MHz**
- Kunming **1.4 GHz**

Thank you

- *"A simultaneous X-ray and radio observation of the nearby pulsar B1133+16" (146ks, XMM-Newton, Gil et. al)*
- *"Study of the remarkable X-ray variability of PSR B0943+10" (300 ks, XMM-Newton, Mereghetti et. al)*

A rapid global transformation of the pulsar magnetosphere?

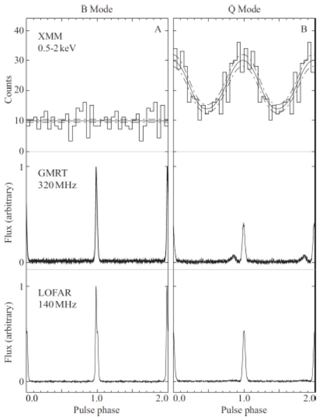

Figure: Aligned X-ray and radio pulse profiles of PSR B0943+10 in its B- and Q-modes *(Hermsen et al. 2013)*.

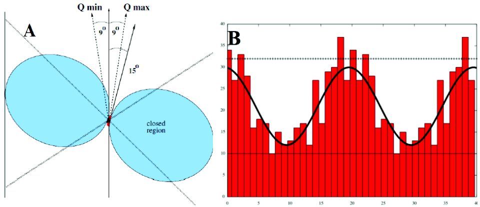

Spectral parameters (see Table S4 in *(Hermsen et al. 2013)*)

Mode	Model	T_s (MK)	$R_{\rm BB}$ (m)	PL	$\chi^2_{\rm red}$/dof.
Q total	BB+PL	3.2 ± 0.5	22 ± 9	2.6 ± 0.3	0.81/20
Q pulsed	PL	–	–	2.5 ± 0.4	3.17/3
Q pulsed	BB	3.7 ± 0.1	33 ± 4	–	0.38/3
B total	PL	–	–	2.3 ± 0.2	0.88/10
B total	BB	2.7 ± 0.2	22 ± 11	–	0.74/10

Preliminary results: Day 1 (x-ray/radio coverage)

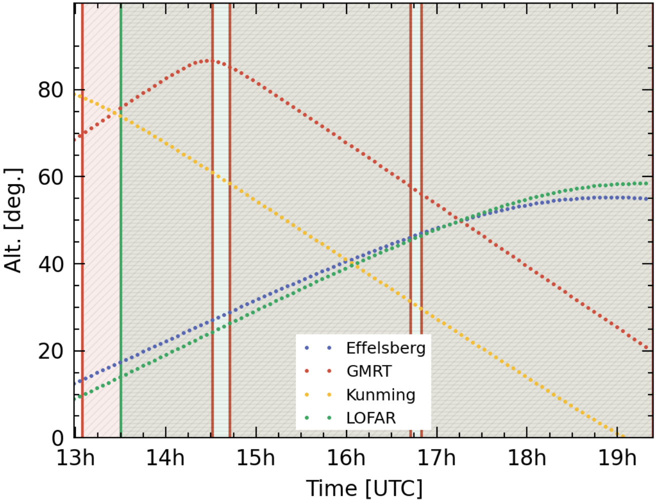

No Effelsberg observation (VLBI session), Kunming data not yet included in the figure.

Preliminary results: Day 1 (x-ray background counts)

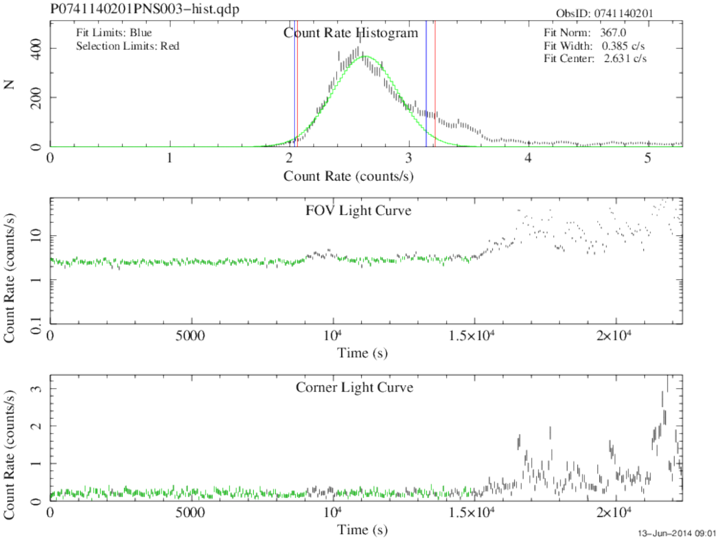

Preliminary results: Day 2 (x-ray/radio coverage)

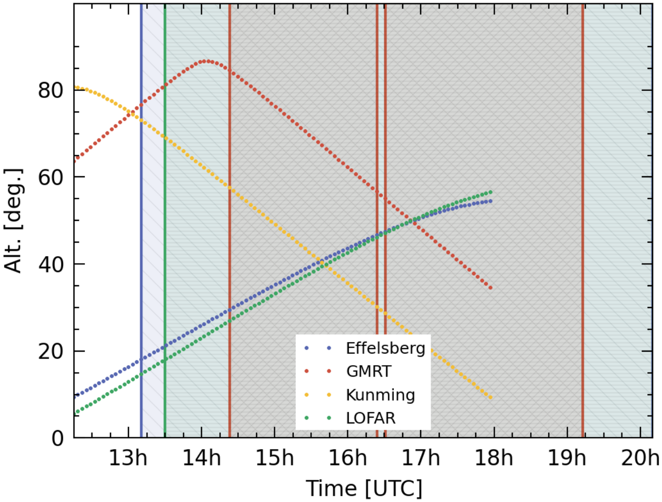

GMRT start delayed due to correlator malfunction, Kunming data not yet included in the figure.

Preliminary results: Day 2 (x-ray background counts)